Synthesis and characterization of poly(carboxymethyl)-cellulose for enhanced La(III) sorption

Ahmad A. Tolba, Said I. Mohamady, Shimaa S. Hussin, Takaya Akashi, Yuka Sakai, Ahmed A. Galhoum, Eric Guibal

Synthesis and characterization of poly(carboxymethyl)-cellulose for enhanced La(III) sorption

Ahmad A. Tolba [a], Said I. Mohamady [a], Shimaa S. Hussin [a], Takaya Akashi [b], Yuka Sakai [b], Ahmed A. Galhoum [a,b,c,**], Eric Guibal [c,*]

[a] Nuclear Materials Authority, P.O. Box 530, El-Maadi, Cairo, Egypt
[b] Hosei University, Faculty of Bioscience and Applied Chemistry, Japan
[c] Ecole des mines d'Alès, Centre des Matériaux des Mines d'Alès, 6, Avenue de Clavières, F-30319 Alès Cedex, France

A B S T R A C T

The grafting of amino and carboxylic acid groups on cellulose increased La(III) sorption efficiency of cellulose: maximum sorption capacity increased from 38 mg La g^{-1} for cellulose to 101 and 170 mg La g^{-1} for amino derivative (PAC) and amino-carboxylic derivative (PCMC). Langmuir equation successfully fits sorption isotherms while uptake kinetics are effectively modeled using the pseudo-first order rate equation (though resistance to intraparticle diffusion plays a significant role in the control of metal recovery). Uptake equilibrium occurred within 150–180 min. The thermodynamic study shows that the reaction is spontaneous, endothermic and entropic. Nitric acid solutions (0.5 M concentration) can be efficiently used for metal recovery and sorbent can be recycled for at least 5 cycles with limited decrease in sorption performance for the three sorbents. The materials were characterized by elemental analysis, acid-base titration, FTIR spectrometry, x-ray diffraction analysis, X-ray photoelectron spectroscopy, SEM-EDX analysis and also by TGA.

Keywords:
Cellulose
Polyaminated cellulose
Poly(carboxymethylation) of cellulose
Lanthanum sorption
Sorption isotherms
Uptake kinetics
Desorption
Thermodynamics
XRD
FTIR
SEM
TGA

1. Introduction

The demand on precious and strategic metals (including rare earth elements, REEs) is tremendously increasing due to the development of electronic and communication devices that contain significant amounts of these metals. The rarefaction of the primary resource, the geopolitics issues (making available or restraining the access to the resource may be a "political weapon" at the world level) can explain that the recovery of these strategic metals from low-level streams and their recycling from waste materials (including spent catalysts and wastes of electric and electronic equipment, WEEEs) became a critical issue for High-Tech industry (catalysis, telecom industry, solar cell, optical glass, special ceramics, superalloys, supermagnets and nuclear industry, etc.) (Charalampides, Vatalis, Apostoplos, & Ploutarch-Nikolas, 2015). The recycling of REEs metals from waste materials is usually including a series of steps such as: (a) grinding, (b) gravimetric (plastics/metals) and magnetic (ferrous/non-ferrous metals) separations, (c) leaching (mainly using acidic solutions) and (d) separation/concentration (Binnemans et al., 2013; Borra, Pontikes, Binnemans, & Van Gerven, 2015; Sinha, Abhilash, Meshram, & Pandey, 2016). Alternative process may use pyrometallurgy (just after gravimetric/magnetic separation). In the present study the sorbents are considered to be used for the recovery of REEs elements processing from hydrometallurgical route.

* Corresponding author.
** Corresponding author at: Nuclear Materials Authority, P.O. Box 530, El-Maadi, Cairo, Egypt.
E-mail addresses: ibn_ata@yahoo.com (A.A. Tolba), said_mohamady75@yahoo.com (S.I. Mohamady), mash_1997@yahoo.com (S.S. Hussin), akashi@hosei.ac.jp (T. Akashi), yukaji_sakai1@yahoo.co.jp (Y. Sakai), Galhoum_nma@yahoo.com (A.A. Galhoum), eric.guibal@mines-ales.fr (E. Guibal).

The recovery of metal ions, and more specifically REEs, can involve many different processes depending on the concentration of valuable or toxic metals, the composition of the solution and the economics of the process and target metals. Solvent extraction is efficiently used for the recovery of REEs from concentrated solutions (Hou, Xu, Wang, & Chen, 2016; Tunsu, Petranikova, Ekberg, & Retegan, 2016; Vander Hoogerstraete & Binnemans, 2014). However, the process may have serious environmental drawbacks (related to extractant/solvent release in water bodies) and limited competitiveness when the metal concentration is relatively diluted (lower than 0.5–1 g L^{-1}). Actually the limit concentration for competitive solvent extraction of metal ions strongly depends on the quotation of the target metal, the complexity of the solution and the objective of the process (separation *vs* simple metal recovery), the final valorization step (precipitation vs. electro-winning), etc. (Lo, Baird, & Hanson, 1991). In the case of lanthanum recovery from leachates, solvent extraction was operated using Cyanex 923 with La(III) amounts ranging between 400 and 800 mg La kg^{-1} (Tunsu et al., 2016). Alternative processes may use precipitation (Martsul & Kozlowskaya, 2015; Sinha et al., 2016); however, this method is rarely selective and huge amounts of multi-metal contaminated sludge are produced, which are sometimes difficult to valorize. Ion-exchange and chelating resins are more appropriate for concentrating and separating metals ions from dilute effluents, playing with the affinity of their specific functional groups of REEs (Esma, Omar, & Amine, 2014; Jain, Handa, Pandya, Shrivastav, & Agrawal, 2002; Jain, Pandya, Pillai, Agrawal, & Kanaiya, 2007; Maheswari & Subramanian, 2004). Extractant impregnated resins offer a compromise between solvent extraction and resin systems and combine the advantages of the two techniques (Baba, Kubota, Kamiya, & Goto, 2011; Karnio, Fujiwara, Mats Urnoto, Valenzuela, & Kondo, 2008; Karve & Rajgor, 2008; Nishihama, Kohata, & Yoshizuka, 2013; Sun, Chi-Linh, Luo, & Dai, 2014; Sun, Ji, Chen, & Ma, 2009): (a) confinement and reliability of resin supports and (b) selectivity/efficiency of solvent/extractant systems. However, for the last decades numerous studies on metal biosorption have been inspired by the ion-exchange and chelating systems for mimicking conventional resins using biomass that bear similar reactive groups for metal recovery from dilute solutions (Cadogan, Lee, Popuri, & Lin, 2014; Das & Das, 2013; Koto, Kano, Wang, Sakamoto, & Imaizumi, 2010; Lo, Cheng, Han, Chen, & Chang, 2014; Oliveira, Guibal, & Garcia, 2012; Song, Park, Kang, Park, & Han, 2013; Wu, Zhang, Wang, Zhu, & Fan, 2011). These renewable resources are usually cost-effective, abundant and they can be used as produced or chemically modified for improving sorption performance (Galhoum et al., 2015a; Galhoum et al., 2015b; Hakim, Sabarudin, Oshima, & Motomizu, 2007; Inoue, Ohto, Yoshizuka, Shinbaru, & Kina, 1995; Repo, Warchol, Bhatnagar, Mudhoo, & Sillanpaa, 2013; Roosen & Binnemans, 2014; Roosen, Spooren, & Binnemans, 2014).

In an attempt to produce performant and cost-effective sorbents for the recovery of lanthanum (as an example of light REEs) from dilute solutions cellulose has been chemically modified first by chlorination for immobilization of polyamine (synthesis of poly(aminated) cellulose, PAC), followed by grafting of carboxyl groups (synthesis of poly(carboxymethyl) cellulose, PCMC). The different materials were extensively characterized using SEM/SEM-EDX analysis, XRD analysis, thermogravimetric analysis, FTIR spectrometry and elemental analysis. The sorption properties of the two derivatives have been compared to those of raw cellulose through the study of pH effect, the analysis of uptake kinetics and the determination of sorption isotherms at different temperatures (in order to calculate thermodynamic parameters). Finally, the metal desorption was investigated for evaluating the possibility to recycle the sorbent.

2. Material and methods

2.1. Reagents

Microcrystalline cellulose $(C_6H_{10}O_5)_n$, (Merck, Germany), tetraethylenepentamine (TEPA), monochloroacetic acid ($ClCH_2CO_2H$) and thionyl chloride ($SOCl_2$) were obtained from Sigma-Aldrich (France) and *N,N*-dimethylformamide (N,N-DMF), 1,4-dioxane (99.9%) and ethanol were supplied by Fluka Chemicals (Switzerland). All other chemicals were Prolabo products (France). These reagents were used as received.

Lanthanum stock solution was prepared from La_2O_3 salt, supplied by Merck (Germany), dissolved in concentrated hydrochloric acid under heating and finally diluted in demineralized water (concentration: 1000 mg La L^{-1}). The working solutions were prepared by appropriate dilution of the stock solution immediately prior to use. The metal concentrations in both initial and withdrawn samples were determined by an Inductively Coupled Plasma Atomic Emission Spectrometer (ICP-AES JY Activa M, Jobin-Yvon, Longjumeau, France).

2.2. Synthesis of cellulose derivatives

Fig. AM1 (see Additional Material Section) shows the schematic route for the synthesis of poly(carboxymethyl) cellulose (PCMC) and its precursor (poly(aminated) cellulose, PAC). Tetraethylenepentamine (TEPA) was grafted on cellulose in two steps. First, cellulose was chlorinated by reaction with thionyl chloride: cellulose (2 g) was suspended in 50 mL of N,N-DMF and progressively heated to 353 K, under stirring for 1 h. When the temperature of the suspension reached the target temperature, 7 mL of $SOCl_2$ was gradually added to the suspension. The reaction being exothermic, the addition was progressive to keep the temperature between 368 and 373 K. The stirring was maintained at the same temperature for 4 h after the reagent was totally added to the suspension. The reactor was then cooled to room temperature and the suspension was poured into 100 mL of iced water under strong agitation. The formed precipitate was filtered, washed with water, and treated with 100 mL of 3% (w/w) NH_4OH (to remove residual sulfurous acid). The product (i) (chlorinated cellulose) was filtered off and extensively washed successively with ethanol and MilliQ water to remove any residual reagents (Silva Filho et al., 2013; Tashiro & Shimura, 1982). In the next step, the product (i) was suspended in 20 mL ethanol before adding 12 mL of tetraethylenepentamine (TEPA), and the mixture was stirred under reflux for 8 h (Mahfouz et al., 2015): the product (ii) (poly(aminated) cellulose, PAC) was recovered by filtration and extensively washed. In the last step, the product (ii) was suspended in N,N-DMF or dioxane (25 mL), before adding 14 g of monochloroacetic acid; the pH of the suspension was adjusted to 9–9.5 with 1 M NaOH solution and heated under reflux for 10 h (Galhoum, Atia, et al., 2015c; Galhoum et al., 2015a; Galhoum, Mahfouz et al., 2015). The final product (iii) (PCMC, poly(carboxymethyl) cellulose) was filtered and washed 3 times with ethanol and MilliQ water. Finally, the sorbents were freeze-dried for 24 h.

2.3. Characterization of materials

The elemental analysis was performed on a Micro Corder JM10 (J-Science Lab Co., Ltd., Kyoto, Japan). The FT-IR spectra were directly obtained without KBr pelletizing within 4000–400 cm^{-1} with a JASCO-FT-IR-6600 spectrometer, Japan. X-ray diffraction (XRD) patterns were obtained at room temperature in the range $2\theta = 10–80^\circ$ using a SmartLab X-Ray Diffractometer

(RIGAKU, Tokyo, Japan), with Cu K_α radiation. TG/DTA had been carried out using a thermogravimetric and differential thermal analyzer EXSTAR 6000 TG/DTA 6300N (Seiko Instruments Inc. (SII) Japan), under N_2/O_2 atmosphere, within the temperature range 293–1173 K with a ramp rate of 20 K/min. The material analysis and the morphology of sorbents were investigated with an ultra-high resolution FE-SEM SU8020 microscope equipped with an energy-dispersive X-ray spectrometer SEM-EDX (Hitachi, Tokyo, Japan) (without liquid N_2); the samples were prepared by adhesion on a carbon film plate and sputter coated with a thin layer of platinum to impart conductivity for incident electrons. X-ray electron spectroscopy was carried out using a X-ray phototoelectron spectrometer (ESCA-5600, Japan) with a 200 W Mg K_α (Al K_α) radiation source; the diameter of X-ray beam was 0.8 mm while the analysis diameter was 1 mm. The samples were adhered on an indium sheet.

The amine content in the sorbents was estimated using a volumetric method (Galhoum et al., 2015b): 50 mL of 0.05 M HCl solution was added to 0.1 g of sorbent under agitation for 15 h. Residual HCl concentration was estimated by titration against 0.05 M NaOH solution (phenolphthalein as the indicator). The number of moles of HCl having interacted with amino group and consequently the amino group concentration (mmol g^{-1}) was calculated from Eq. (1):

$$\text{Concentration of amino group} = (\text{M1}-\text{M2})\,50/0.1 \quad (1)$$

where M1 and M2 are the initial and final concentrations of HCl, respectively. The carboxylate content was also determined by titration using the same concept but inverting the titrants.

2.4. Sorption tests

Batch experiments were carried out by contact of 0.02 g of sorbent (m) with 100 mL of aqueous solution (volume V, L) at given initial metal concentration (C_0: 100 mg La L^{-1}) in a closed flask under agitation (300 rpm) and at 300 K for 4 h. The final pH was recorded in the filtrate and the residual metal concentration in the aqueous phase (C_{eq}, mg La L^{-1}) was estimated by ICP-AES (inductively coupled plasma atomic amission spectrometer, Horiba Jobin-Yvon Activa M, Longjumeau, France), whilst the concentration of metal ions sorbed onto the sorbent (q_{eq}, mg La g^{-1}) was obtained by the mass balance equation, (Eq. (2)):

$$q_{eq} = (C_0 - C_{eq}) \times V/m \quad (2)$$

Standard experimental conditions were set at T: 293 ± 1 K and pH: 5.00 ± 0.01; the contact time was fixed to 3 h. However, when relevant, these parameters were varied for determining pH effect, sorption isotherm characteristics and uptake kinetics.

Isotherm studies were investigated by mixing 0.02 g of sorbent with 100 mL of La(III) solution at different initial concentrations (i.e., 25, 50, 75, 100, 150 and 200 mg La L^{-1}, at pH 5) and shaking for 3 h at 200 rpm. The experiments were performed in a thermostatic chamber, at different temperatures (293 K, 300 K, 313 K and 323 K, maximum temperature variation around target value: ± 2 K).

Uptake kinetics were performed using a sorbent dosage of 0.2 g L^{-1} and a concentration of 100 mg La L^{-1} at 300 ±1 K; samples were collected under agitation at standard times and metal concentration was determined, after filtration, by ICP-AES.

The investigation of desorption process was performed by mixing for 60 min the metal-loaded sorbent with 0.5 M HNO_3 solution (at 297 K; sorbent dosage: 0.1 g L^{-1}). Lanthanum concentration in the filtrate was analyzed by ICP-AES and the mass balance equation was used for calculating at each step the desorption efficiency. The recycling of the sorbent was evaluated by repeating the sorption step and comparing residual concentrations and sorption capacities. The loading of lanthanum on the resins was obtained by contact under agitation of the sorbent with a 100 mg La L^{-1} solution (sorbent dosage 0.2 g L^{-1}) for 3 h at a temperature of 297 K. The recycling of the sorbents was evaluated by comparing the sorption capacities at the successive steps in a series of 6 cycles of sorption/desorption. The duplication/triplication of selected experiments showed that the standard deviation was less than 6–7%.

The modeling of sorption isotherms and uptake kinetics was carried out using conventional models such as the Langmuir (Langmuir, 1918), Freundlich (Freundlich, 1906) and Dubinin-Radushkevich models (Dubinin, Zaverina, & Radushkevich, 1947) (for sorption isotherms) (Foo & Hameed, 2010), the pseudo-first order rate equation (PFORE, (Lagergren, 1898), the pseudo-second order rate equation (PSORE, Ho & McKay, 1999) and the Weber & Morris simplified model for resistance to intraparticle diffusion (sRIDE, Weber & Morris, 1963). The detailed presentation of these models is shown in Additional Material Section.

3. Results and discussion

3.1. Synthesis of materials and characterization of sorbents

The chemical modification of cellulose can be followed comparing the elemental analysis of the product (CHN analysis) at the different stages of the process (Table AM1, see Additional Material Section). After chlorination the fraction of C and H elements deceases due to the grafting of thionyl chloride and to the impact of Cl element in the final product. By analogy with the phosphorylation of cotton cellulose using phosphoryl chloride (Vigo & Welch, 1974), the reaction of thionyl chloride is useful for immobilizing chloride groups, which are reactive for further immobilization of amine-bearing reagents (da Silva Filho, de Melo & Airoldi, 2006; da Silva Filho, de Melo, da Fonseca & Airoldi, 2009; Tashiro & Shimura, 1982). After reaction with tetraethylenepentamine (TEPA) the proportion of C and H elements increases due to the immobilization of the organic moiety; nitrogen content reaches 5.73 mmol N g^{-1} (8.02%, w/w): this means that the grafting of TEPA on cellulose is very efficient. This also means that the TEPA molar fraction content in PAC reaches 1.146 mmol g^{-1}. Assuming the structure of the PAC shown in Fig. AM1 (see Additional Material Section), the substitution of TEPA on cellulose chain is close to 1 TEPA every 2–3 cellulose units. XPS analysis of the three materials shows that poly(amination) is followed by the appearance of two peaks characteristics of N_{1s} (at BE: 401–402 eV) and N_{KLL} signals on PAC, while their intensities are slightly decreasing after poly(carboxymethylation) in PCMC (Fig. AM2, see Additional Material Section). Similar appearance of N_{1s} signals were observed after grafting imidazole on cellulose through glycidylmethacrylate bridging (O'Connell, Aszalos, Birkinshaw, & O'Dwyer, 2010). It is noteworthy, that insufficient washing or uncomplete substitution led to the presence of a small amount of chloride on PAC and PCMC sorbents (presence of the Cl_{2p} signal). The detailed XPS spectra around the typical C_{1s}, N_{1s} and O_{1s} signals show characteristic shifts of the BEs that can be directly associated to changes in the environment of these elements due to chemical grafting of new groups (Stenstad, Andresen, Tanem, & Stenius, 2008). A small shift of the peak for (N_{1s}) and the appearance of a more marked shoulder (around 400 eV) are observed after carboxymethylation, which is also illustrated by the broadening of the shoulder around 532 eV which is attributed to C—O and COO groups (Ye, Wang, Xiong & Sun, 2016): This is the convolution of two signals that represent C═O groups and C—OH/C—O—C groups at around 531.7 eV and 533.2 eV, respectively (Shen et al., 2013; Ye et al., 2016): this confirms the grafting of carboxylic groups on cellulose backbone. After chemical grafting of TEPA on nitric acid-oxidized carbon fibers the XPS spectra showed that apart the appearance of the N_{1s} signal a decrease

of the relative concentration of C—OH groups (around 533 eV) was observed (O_{1s} signal) together with a broadening of the C_{1s} peak (at 284 eV) (Gardner, Singamsetty, He, & Pittman, 1997).

The grafting of carboxylic acid groups on TEPA-functionalized cellulose occurs by reaction of monochloroacetic acid with amine groups of TEPA and HCl release. This is confirmed by the decrease of the pH of the suspension from 9.3 to 3.7 during the reaction (requiring continuous pH control). Nitrogen content decreases from 10.86% (w/w) (i.e., 7.75 mmol N g^{-1}) to 8.10% (w/w) (i.e., 5.78 mmol N g^{-1}) after poly(carboxylation) of TEPA-functionalized cellulose (PAC); this shows the efficient carboxymethylation in the PCMC material: the molecular weight of the final derivative strongly increases and then "dilute" N element in the final product. A simulation on the effect of the degree of substitution on amine groups on the relative mass fraction of N element in the final product demonstrates that the reaction of monochloroacetic acid is almost quantitative.

The acid-base titration of PAC and PCMC (Galhoum, Mahfouz et al., 2015) showed that the amine contents were close to 7.61 mmol —NH g^{-1}, and 4.73 mmol —NH g^{-1}; respectively. On the other hand the titration of carboxylic groups in PCMC (corrected by the amount of alkaline titrant consumed by titration of amine groups of PAC) showed a carboxylic acid content in the sorbent close to 8.74 mmol g^{-1}. It is noteworthy that the ratio of carboxylic groups in PCMC to amine groups in PAC (molar units) is close to 1.15; this means close to the expected molar ratio assuming the substitution reaction to be complete (i.e., 1.2). These results confirm the efficiency of the successive reactions of chlorination, poly(amination) and poly(carboxymetylation).

The Fourier-transform infrared spectrometric analysis of the different samples confirms the synthesis route (Fig. AM3, see Additional Material Section). Microcrystalline cellulose is characterized by typical bands at 3600–3100 cm^{-1} (a broad band that corresponds to –OH stretching vibration) and 2900 cm^{-1} (C—H stretching vibration).

However, these bands are poorly resolved and can be difficultly used for identifying the products; more interesting is the interpretation of the spectrum in the wavenumber range 1800–500 cm^{-1}. The small band at 1638 cm^{-1} corresponds to the deformation vibration of hydroxyl groups. The bands at 1427 cm^{-1} and 1365 cm^{-1} were assigned to CH_2 symmetric bending (at C-6) and C—H bending, respectively (Oh et al., 2005). The frequency at 1314 cm^{-1} can be assigned to CH_2 wagging deformation at C6, while the small peak close to 1282 cm^{-1} is attributed to C—H deformation mode (Oh et al., 2005). The band at 1202 cm^{-1} (doubled by another band at 1236 cm^{-1}, poorly resolved) is assigned to the deformation mode of C—OH in plane at C-6. The bands at 1159 cm^{-1} and 1051 cm^{-1} are assigned to C—O—C stretching mode (at β-glycosidic linkage) and to the stretching vibration modes of C—O at C-3 and/or of C—C (Oh et al., 2005). The in plane deformation mode for the carbohydrate ring is identified by the peak at 1105 cm^{-1}.The stretching modes for C—O at C-6 are characterized by two bands at 1027 cm^{-1} and close to 1000 cm^{-1}. The peak at 896 cm^{-1} may be assigned to several stretching vibrations corresponding to C—O—C, C—C—O and C—C—H bonds (Ciolacu, Ciolacu & Popa, 2011; Oh et al., 2005). The peak at 661 cm^{-1} is attributed to the out of plane bending mode of the C—OH bond. After chlorination two bands are appearing at 749 cm^{-1} and 721 cm^{-1}, corresponding to stretching vibration of C—Cl bond (Silva Filho et al., 2013). On the other hand, the band at 896 cm^{-1} was shifted down to 867 cm^{-1}. A new weak band is also appearing at 1727 cm^{-1}; this band is difficult to explain on the basis of suggested mechanism since this wavenumber usually corresponds to carboxylic groups (Coates, 2000). This band is not appearing in the chlorination of cellulose for the synthesis of sulfur derivatives of cellulose (Silva Filho et al., 2013). After TEPA grafting the two bands attributed to cellulose chlorination (i.e., 749 and 721 cm^{-1}) disappear; the band at 866 cm^{-1} (corresponding to the shift of C—OH stretching of cellulose) also disappears. These changes in FTIR spectrum are consistent with results obtained in the grafting of ethylenediamine on chlorinated cellulose (Silva Filho et al., 2013). This confirms the successful reaction of polyamine on chlorinated groups. The efficient polyamination of cellulose is also demonstrated by the strong peak appearing at 1647 cm^{-1}, which can be assigned to N—H bending vibration in primary and secondary amine groups (Coates, 2000). The enlargement of the band at 1010–1050 cm^{-1} may be explained by the increase in the intensity of the peak at 1042 cm^{-1}, which is assigned to the N—H stretching vibration of primary and secondary amine groups. After monochloroacetic reaction (PCMC) the main changes appearing on FTIR spectrum concern: (a) the enlargement of the band at 1639 cm^{-1}, and (b) the increase in the intensity of the peak at 1387 cm^{-1}. These bands are generally poorly selective being identified in many bonds; however, they can probably be assigned to carboxylate functional groups (Coates, 2000). These results are consistent with previous elemental analysis and acid-base titration characterization for confirming the synthesis route.

X-ray diffraction analysis of raw cellulose (Fig. AM4, see Additional Material Section) shows the typical peaks of cellulose I at $2\theta = 15.1$, 16.4, 22.6 (Krishnaveni & Thambidurai, 2011; Liu & Zhang, 2009; Oh et al., 2005; Silva Filho et al., 2013). These peaks correspond to $1\bar{1}0$, 110, 020 lattice planes of cellulose I (Isogai, Usuda, Kato, Uryu, & Atalla, 1989). After chemical modification the change in the structure of the biopolymer (hydrogen bonds replaced with other bonds like C—Cl, C—N, etc.) is reflected by the change in the crystallinity; instead of the relatively well-resolved of microcrystalline cellulose the XRD patterns of PAC and PCMC are characterized by an amorphous pattern (Park, Baker, Himmel, Parilla & Johnson, 2010; Silva Filho et al., 2013). The drastic change in the pattern after chemical modification (associated to the disappearance of the typical peaks of microcrystalline cellulose) makes meaningless the calculation of the crystalline index for PAC and PCMC. Silva Filho et al. followed the appearance of an additional crystallinity (new diffraction plans) after cellulose chlorination: hydroxyl groups on amorphous parts of cellulose are replaced by chlorine atoms (Silva Filho et al., 2013). After reaction with ethylenediamine the polymer completely loses its crystallinity (consistently with the present results). Silva Filho et al. assume that the reaction of the amine compound with chlorinated cellulose contributes to the disruption of the inner and intramolecular bonds in the material: these interactions are responsible of the structural organization and crystallinity of the original biopolymer. While grafting the organic substituent the disorder of the material is strongly increased (especially with the intercalation of large molecules: the effect of TEPA is expected to be stronger than that of ethylenediamine) and the material becomes amorphous.

Thermogravimetric analysis (under N_2/O_2 conditions) shows that the chemical modification of microcrystalline cellulose strongly affects the degradation profile of the materials (Fig. AM5, see Additional Material Section). Cellulose degradation follows a simple degradation profile formed of 5 steps: (a) loss of absorbed water (about 4%, w/w), (b) almost stable plateau (till 553 K), (c) sharp weight decrease (with the highest rate of weight loss close to 593 K, given by the TDG), (d) slower phase of thermal degradation (from 623 K to 813 K, which represents a weight loss of 12%), and (e) the final plateau that corresponds to the complete degradation of cellulose. The strong weight loss (about 85%) occurring around 595 K corresponds to the thermal decomposition of the cellulose while the second phase (slower slope) corresponds to the complete combustion of the organic residue (under N_2/O_2 atmosphere). For PAC and PCMC the degradation profiles are also characterized by 5 steps: (a) weight of water absorbed in the biopolymer, (b) fol-

lowed by a progressive loss of weight (representing 10% for PAC and 17% for PCMC) till 463 K, (c) sharp decrease of weight around the maximum loss rate at 513 K that represents less than 30%, (d) a progressive weight loss with a lower slope till reaching 873–903 K, (e) final step with complete degradation of PCMC while for PAC the residual amount is close to 3%. Similar increase in the stability was reported for ethylene sulfide grafting on cellulose (Silva Filho et al., 2013). In the case of chlorinated cellulose Silva Filho et al. reported the release of surface-adsorbed water in the range 386–430 K followed by the displacement of HCl molecule and the condensation of the hydroxyl groups on C-2 and C-3 between 438 and 534 K, and the final decomposition of cellulose fibers above 521 K (da Silva Filho et al., 2006). After the grafting of ethylenediamine moiety the thermal degradation profile was very close to the profile obtained for chlorinated cellulose: the decomposition of the ethylenediamine substituent was identified in the range 364–563 K. With PAC and PCMC the profiles are very similar and close to the profiles obtained by da Silva Filho et al. (2006); though the decomposition was performed under N_2/O_2 atmosphere (contrary to N_2 atmosphere). The first event corresponds to a weak weight loss attributed to water adsorbed at the surface of the sorbent, followed by a progressive weight loss representing 10–17% and that could be attributed to the loss of polyamine (for PAC and PCMC) and carboxylic groups (for PCMC) (identified by DTG peak at 513 K). In the next step the cellulose backbone is decomposed and finally completely burned (at a higher temperature than for microcrystalline cellulose; i.e., 877–903 K against 796 K).

It is noteworthy that these materials may have a significant advantage against more conventional resins when considering the complete life-cycle of the sorbents. Indeed, at the end of life cycle the thermal degradation of synthetic resins (for example) may produce hazardous sub-products, such as toxic volatile compounds (Dubois, Dozol, Nicotra, Serose, & Massiani, 1995). The changes in the slopes and the different breakdowns in the degradation curves can be correlated to the presence of the substituents, which have their own thermal degradation patterns. Similar modifications of thermal degradation profiles were reported in the case of chemical modification of cellulose by grafting of aldehyde and carboxyl groups (Sharma & Varma, 2014).

Scanning electron microscopy was used for characterizing the morphology of sorbent particles (Fig. AM6, see Additional Material Section). Cellulose shows a fibrillary structure while cellulose derivatives are characterized as small agglomerates of micro-size flaked particles (100–200 nm). Fig. AM7 (see Additional Material Section) shows the SEM-EDX analysis of the samples including their EDX spectra and the cartographies of the distribution of O element (tracer of cellulose backbone and poly(carboxylation)) and N element (tracer of poly(amination)). In the case of cellulose the tracers are C and O elements and the distribution of elements appear homogeneous: the gradients can be directly correlated to the topographic changes (height of the sample and possible shadow effect). The distribution of N elements (which is representative of polyamination of cellulose) appears homogeneous in the cartography of PAC (as is the distribution of O element, tracer of cellulose backbone). The N element is homogeneously distributed at the surface of PCMC particles: the grafting of DETA is thus expected to be homogeneous. The O element is present on both cellulose backbone and as the result of carboxylation of amine groups (reaction of monochloroacetic acid): it is not possible to identify their respective contributions but the distribution of O element appears also homogeneous; though the analysis is not quantitative the density of O element is higher than in Cellulose sample. This is consistent with the interpretations made in the elemental analysis of the sorbents, where the carboxylation reaction was considered as almost quantitative: carboxylic groups are homogeneously distributed (similarly to amine groups, and N element).

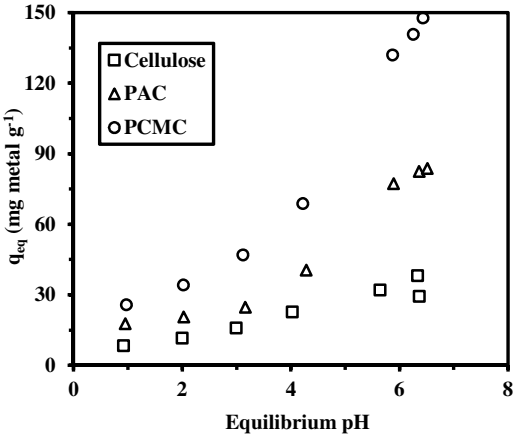

Fig. 1. Effect of pH on La(III) sorption using Cellulose, PAC and PCMC (C_0: 100 mg La L^{-1}; T: 300 K; contact time, t: 3 h; sorbent dosage, SD: 200 mg L^{-1}; initial pH values: 1.01, 2.00, 2.99, 3.99, 5.02, 6.01 and 6.98, respectively, See Fig. AM8, Additional Material Section for pH variation during metal sorption).

3.2. *pH effect on La(III) sorption*

The pH has a critical impact on La(III) sorption (Fig. 1). The sorption capacity progressively increases with pH for cellulose, while for both PAC and PCMC two regions can be identified: (a) a preliminary pH range (between 1 and 3) with a slight increase in sorption capacity and (b) above pH 3 a strong increase in sorption capacity. For PAC the sorption levels remain very close to the values reached with cellulose at pH below 3. Cellulose sorbent (used as the reference) is able to bind metal cations through hydroxyl groups while cellulose derivatives are offering numerous different groups: primary and secondary amine groups for PAC and carboxylic groups and tertiary amine groups (Fig. AM1, see Additional Material Section). This sigmoidal shape of the q-pH curve was also reported in the binding of REEs using EDTA- and DTPA-chitosan derivatives supported on silica particles through sol-gel process (Roosen et al., 2014).

The acid-base properties of these specific groups are important parameters for the interpretation of pH effect on metal sorption. Indeed, protonation/deprotonation reaction affect the affinity of these reactive groups for metal cations that can be bound on (a) carboxylate groups by chelation and/or ion exchange (exchange of protons with metal cations), or on (b) deprotonated amine groups by chelation on the free electron doublet of nitrogen (in amine groups). Depending on the pH and the protonation of these reactive groups the different binding mechanisms can be operative or not. In the case of PAC the TEPA immobilized on cellulose brings primary and secondary amine groups with intrinsic acid-base properties; although these acid-base properties are affected by the grafting on cellulose backbone the pK_a values of the 5 amine groups are reported to be close to 3.36, 4.92, 8.22, 9.23 and 9.80 (values at low ionic strength, increasing the ionic strength slightly shifts pK_a values toward higher values; ΔpK_a: 0.2–0.3), respectively (De Stefano, Foti, Gianguzza, & Sammartano, 2000). As a consequence the deprotonation of amine groups will occur at pH higher than 3.4: this can be correlated to the significant increase in sorption capacity of PAC at pH higher than 3. In the case of chitosan aminopolysaccharide the sorption of Eu(III) was also correlated to the progressive deprotonation of amine groups: FTIR analysis confirmed the major contribution of amine groups (with a stabilization effect of hydroxyl groups) (Cadogan, Lee, & Popuri, 2015).

Ozaki et al. already reported the formation of outer spherical complex of amine groups of chitosan (Ozaki et al., 2006). In the case of PCMC, the coexistence of both amine functions and carboxylic groups makes the interpretation relatively more complex. By analogy with carboxymethyl chitosan (Wang, Chen, Liu, Li, & Zhou, 2008), it is possible to identify critical pH values for the deprotonation of carboxylic groups (in the range 2.4–3.1) and amine groups (i.e.; 6.3–7.8): these values were reported for carboxymethyl chitosan and depends on the ionic strength, the degree of substitution of chitosan and the degree of ionization of reactive groups. Obviously the specific values for pK_a values of carboxylic and amine groups in PCMC will be different but these values are indicative of the intrinsic acid-base properties of the cellulose derivative and its deprotonation behavior. At pH above 3 carboxylic groups are deprotonated and carboxylate functions are beginning to bind La(III) cations, on the other hand when the pH increases amine groups are progressively becoming less protonated and both carboxylate and amine sites will be able to bind metal cations. In the case of La(III) on *Pseudomonas aeruginosa*, the binding of the metal ions was associated to peptidoglycans present on the cell wall of the bacteria through a mechanism involving several carboxylate groups and amine groups of different adjacent chains (Texier, Andres, Illemassene, & Le Cloirec, 2000). In the case of La(III) biosorption on *Pseudomonas* sp. the binding mechanisms were attributed to a combination of ion-exchange, complexation and microprecipitation at the surface of the biomass (Kazy, Das, & Sar, 2006). In the case of chemically modified chitosan Eu(III) binding mechanism was attributed to coordination with two nitrogen atoms and three oxygen atoms in the case of EDTA-grafted derivative and with three nitrogen atoms and four oxygen atoms for DETPA (diethylenetriamine pentaacetic acid) (Roosen & Binnemans, 2014). This mechanism is enhanced by the deprotonation of both amine groups and carboxylate groups. Similar mechanisms can be anticipated for La(III) sorption on PCMC. The complexation of lanthanides with tetraethylenepentamine (in DMSO solvent) demonstrated the direct binding of Eu(III) and Tb(III) through amine groups with contribution of solvent molecules (Di Bernardo et al., 2008). As a conclusion the binding of La(III) increases with pH due to the progressive deprotonation of amine and carboxylic groups that can bind metal cations through chelation and/or ion exchange.

The pH can also influence metal speciation through formation of hydroxo-complexes that may change the global charge of La(III); in the presence of soluble ligand this would also affect the chelation of the metal and then its affinity for reactive groups (change in the global charge) and even the binding mechanism and the pH range of optimal sorption (Diniz & Volesky, 2005b; Guzman, Saucedo, Navarro, Revilla, & Guibal, 2002; Guzman, Saucedo, Revilla, Navarro, & Guibal, 2003). In the case of 2 mM La(III) solutions, the calculation of metal speciation using Medusa (Puigdomenech, 2010) shows that the formation of the hydroxo complex $La(OH)^+$ only begins at pH 6.1 while the formation of the precipitate of $La(OH)_3$ only occurs above pH 7.5. This means that under selected experimental conditions, the metal does not precipitate and the hydroxo complex (which represents less than 2–3%) does not really contribute to metal binding. Fig. AM8 (see Additional Material Section) shows pH variation during metal sorption. In the range pH 1–4, pH remains almost constant while in the range 4–6 the pH tends to increase (this is probably associated to proton binding). Above pH 6 the pH tends to decrease in relation with the formation of hydroxo complexes. However, it is noteworthy that the maximum pH variation (ΔpH) does not exceed 0.7 unit.

3.3. Uptake kinetics

Uptake kinetics were compared for the three sorbents (Fig. 2). Very similar profiles are obtained: a fast initial sorption (within the first 50 min of contact) with almost linear increase in sorption capacity (*vs.* time), which represents about 80% of total sorption. The sorption occurs on the very accessible sorption sites located at the surface of sorbent particles; the sorption velocity is enhanced by the high concentration gradient between the solution and the surface (and the internal reactive sites). In the range of contact time 50–120 min, the sorption velocity decreases due to a decrease in the concentration gradient and to the contribution of the mechanism of resistance to intraparticle diffusion. Between 120 and 180 min of contact the sorption continues with very slow velocity due to strong resistance to intraparticle diffusion (to reach the most internal sorption sites through the thinnest pores). The equilibrium plateau is systematically reached within 180 min of contact (at least under selected experimental conditions). These trends are confirmed by the Weber and Morris plots (Fig. AM9, see Additional Material Section): three linear segments are identified corresponding to these three steps and to possible contributions of different diffusion mechanisms due to micro-, meso- and macro-porosities of the sorbents in addition to resistance to film diffusion.

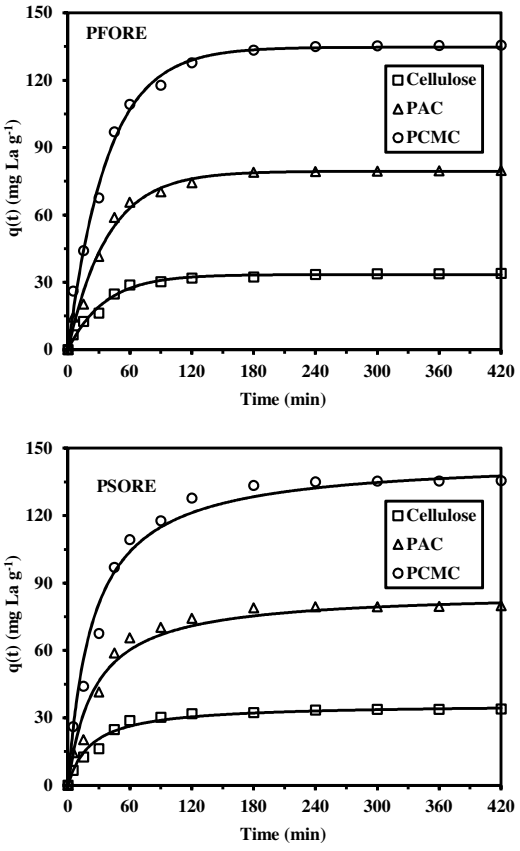

Fig. 2. La(III) uptake kinetics for Cellulose, PAC and PCMC (C_0: 100 mg La L^{-1}; pH: 5; T: 300 K; sorbent dosage, SD: 200 mg L^{-1}) and modeling with the PFORE and the PSORE.

In Fig. 2 the solid lines represent the fitted curves (solid lines) superimposed on experimental data (symbols) for both the PFORE and the PSORE using the model parameters summarized in Table 1. Both models give good fit of experimental data; however, the PFORE achieves a better fit of experimental profiles, especially in the most curved part of the profiles. In addition, the comparison of calculated sorption capacities at equilibrium with experimental values shows that the PSORE systematically overestimates the sorption capacity while the PFORE gives very close values.

This is also consistent with the comparison of determination coefficients (i.e., R^2) that are systematically superior for PFORE than for PSORE. It is noteworthy that the PFORE apparent rate coefficient

Table 1
Kinetic parameters for La(III) sorption using cellulose, PAC and PCMC.

Model parameters		Sorbent		
		Cellulose	PAC	PCMC
Experimental	q_{eq} (exp.) (mg La g^{-1})	34.0	79.9	135.5
PFORE	q_{eq} (calc.) (mg La g^{-1})	33.4	79.5	134.7
	$k_1 \times 10^2$ (min^{-1})	2.83	2.63	2.63
	R^2	0.989	0.991	0.995
PSORE	q_{eq} (calc.) (mg La g^{-1})	37.2	89.2	150.5
	$k_2 \times 10^3$ (g mg^{-1} min^{-1})	1.05	0.38	0.23
	R^2	0.982	0.978	0.987

(i.e., k_1) is almost the same for the three sorbents (in the range $2.63–2.83 \times 10^{-2}$ min^{-1}). La(III) sorption is relatively fast under selected experimental conditions: 150–180 min of contact are sufficient for reaching the equilibrium and the apparent rate coefficient (PFORE) is not significantly affected by the chemical modification of the support (k_1: $2.7 \pm 0.1 \times 10^{-2}$ min^{-1}). It is noteworthy that the rate coefficient for the PSORE tends to progressively decrease with the polyamination and the grafting of the carboxylic acid groups (k_2 decreases from 1.05×10^{-3} to 0.23×10^{-3} g mg^{-1} min^{-1}). The apparent rate coefficients intrinsically take into account the effect of resistance to intraparticle diffusion when applied to heterogeneous systems. This may explain the effect of chemical modification on the PSORE coefficient in relation with the change in crystallinity and the packing of the polymer network. Surprisingly, the decrease in the crystallinity of the material is expected to enhance hydration and mass transfer performance and a contrary trend is observed in the present case. The Weber and Morris plots (Fig. AM9, see Additional Material Section) show an increase in the rate coefficient for intraparticle diffusion on the first two segments according the sequence: PCMC > PAC > Cellulose; this means that the chemical modification is supposed to improve the mass transfer properties. This would be consistent with the re-arrangement of the crystalline structure associated to the insertion of large molecules (confirmed by XRD analysis): microcrystalline cellulose turns to amorphous materials, which, is expected to improve hydration and diffusion properties. However, at the overall level, this is not clearly appearing (almost constant value of k_1).

3.4. Sorption isotherms and thermodynamic analysis

The sorption isotherms have been investigated at 4 different temperatures in order to evaluate thermodynamic parameters, maximum sorption capacities and sorption affinity of the three sorbents for La(III) (Fig. 3). Systematically the sorption capacity increases with temperature: the sorption mechanism is endothermic. The curves are all characterized by a steep initial slope followed by a progressive saturation plateau. This asymptotic form is more consistent with the Langmuir equation than with the Freundlich equation. This is confirmed by the linearization of experimental data with the two models (Figs. AM10 and AM11 for Langmuir and Freundlich equations, respectively; see Additional Material Section) and by the good simulation of experimental data (represented by solid lines in Fig. 3): Langmuir equation perfectly fits experimental data: the determination coefficients are close to 1 (Table 2) and higher than those obtained with the Freundlich equation (Fig. AM11, Table AM2, see Additional Material Section).

Though good mathematical fits do not mean that the hypotheses associated to the model are fulfilled; this is an indication of possible mechanisms involved in metal binding: in the case of Langmuir model the sorption is supposed to occur as a monolayer phenomenon without interactions between sorbed molecules with homogeneous energy of sorption (homogeneous sorption sites).

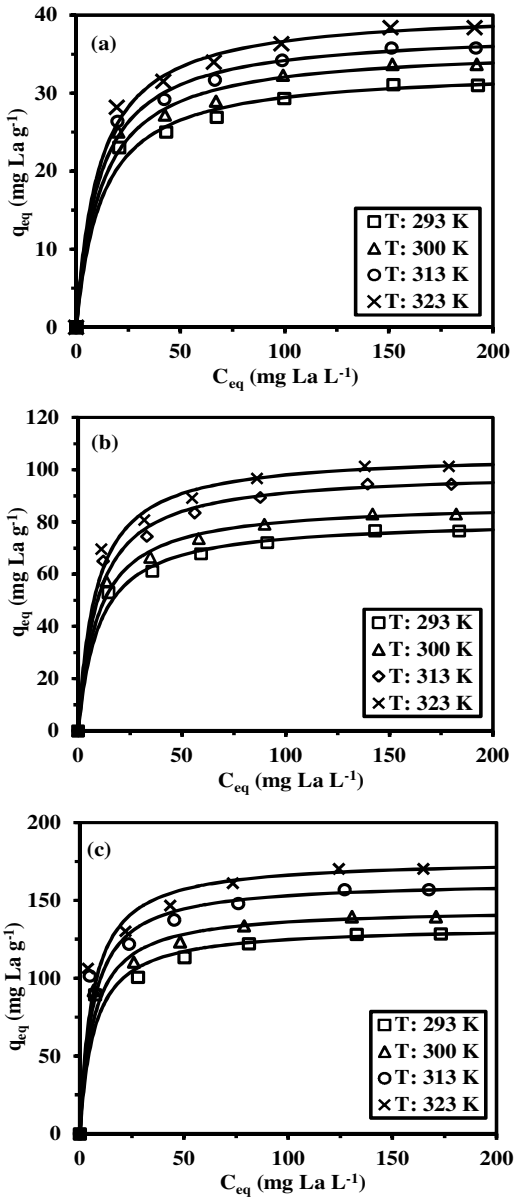

Fig. 3. Effect of temperature on La(III) sorption isotherms using Cellulose (a), PAC (b) and PCMC (c) at pH 5.

The coexistence of different reactive groups (hydroxyl in cellulose and derivatives, amine groups in PAC and PCMC and carboxylate groups in PCMC) does not affect the mathematical fitting of sorption isotherms, despite the diversity and the different affinities of these reactive groups.

Obviously, the maximum sorption capacity increases according the sequence Cellulose < PAC < PCMC. La(III) is considered as a hard acid (low polarizability, forming "hard spheres"; softness parameter: −0.75 (Marcus, 1997)), which is supposed to react strongly and fast with hard bases (Pearson, 1966). La(III) form preferentially complexes with ligand having oxygen as the donor atom. The reaction of monochloroacetic acid on PAC leads to the grafting of numerous carboxylic acid groups, whose, in turn, enhance La(III) sorption. This is consistent with the ranking in affinity coefficients (coefficient b in Table 2) Cellulose < PAC « PCMC. The affinity

Table 2
La(III) sorption isotherms at different temperatures for cellulose, PAC and PCMC – Parameters of the Langmuir equation.

Sorbent	Temp. (K)	q_m (mmol La g^{-1})	q_m (mg La g^{-1})	b (L mg^{-1})	$q_m \times b$ (L g^{-1})	R^2
Cellulose	293	0.238	33.1	0.0811	2.68	0.999
	300	0.259	35.9	0.0829	2.98	0.998
	313	0.274	38.0	0.0898	3.41	0.999
	323	0.293	40.7	0.0905	3.68	0.999
PAC	293	0.583	80.9	0.099	8.00	0.999
	300	0.630	87.6	0.106	9.28	0.999
	313	0.716	99.5	0.109	10.82	0.999
	323	0.766	106.4	0.117	12.45	0.999
PCMC	293	0.961	133.5	0.144	19.16	0.999
	300	1.044	145.0	0.153	22.19	0.999
	313	1.170	162.6	0.160	26.01	0.999
	323	1.271	176.5	0.162	28.61	0.999

Table 3
Comparison of sorption capacity for La(III) ions with selected sorbents.

Sorbent	Initial pH	Time, (min)	Temp. (K)	Sorption capacity, (mg La g^{-1})	Reference
Amine-chitosan magnetic nanobased particles	5	240	320	50.6	Galhoum et al. (2015b)
Activated carbon derived from rice husk	3.5	60	293	175.4	Awwad, Gad, Ahmad, and Aly (2010)
Modified bamboo charcoal	7.2	300	288	192.0	Chen (2010)
			308	214.0	
Sargassum polycystum Ca-loaded biomass	3	1440	–	111.1	Diniz and Volesky (2005a)
	4	1440	–	125.0	
	5	1440	–	138.9	
Iron oxide loaded Ca-alginate beads	2.3	1680		1.9	Wu, Zhao, Zhang, Wu, and Yang (2010)
				98.7	
				119.3	
	3.5		298		
	5				
Grapefruit peel	5	60	–	171.2	Torab-Mostaedi, Asadollahzadeh, Hemmati, and Khosravi (2013)
SnO_2–TiO_2 NCs nanocomposites	5	60	298	65.6	Rahman, Khan, Marwani, and Asiri (2014)
Polydopamine on nanofibrous mats	4.5	1440	298	59.6	Hong et al. (2014)
DTPA functionalized magnetite nanoparticles	6	90	298	62	Almeida and Toma (2016)
Lewatit TP 207 and TP 260 resins	3.6 and 5.2	30	298	114 and 106	Esma et al. (2014)
EHPNA(Extractant) loaded microcapsules	3	10	313	19	Karnio et al. (2008)
Carboxymethyl cellulose based open-cellular hydrogel adsorbent	7	30	303	384.6	Zhu, Wang, Zheng, Wang, and Wang (2016)
Cellulose	5	180	323	38.4	This work
PAC	5	180	323	101.3	This work
PCMC	5	180	323	170.2	This work

–: not clearly mentioned.

coefficient can be also used for calculating the R_L dimensionless constant:

$$R_L = \frac{1}{1 + b \times C_0} \quad (3)$$

when R_L is below 1 the solute binding is usually considered as a "favorable" sorption process. Obviously, for a given system, increasing initial concentration (C_0, mg La L^{-1}) mathematically decreases the value of R_L. These values were calculated for the two extreme initial concentrations (i.e., C_0: 25 and 200 mg La L^{-1}) at the different temperatures: the values of R_L systematically range between 0.05 and 0.33 for Cellulose, between 0.04 and 0.29 for PAC and between 0.03 and 0.22 for PCMC. Obviously the sorption of La(III) on the three sorbents is favorable, the "favorability" increases with metal concentration and is comparable for the three sorbents.

The grafting of new reactive groups on cellulose backbone obviously increases sorption efficiency and capacity. However, it is difficult correlating maximum sorption capacities to the content of these sorbents (molar concentration of amine groups and carboxylic acid groups) since different mechanisms can be involved at molecular level, depending on reactive groups (amine groups *vs.* combined amine/carboxylic acid groups) and their steric arrangement/packing. Acid-base titrations showed 7.61 mmol —NH g^{-1} for PAC and 4.73 mmol —NH g^{-1} plus 8.74 —COOH g^{-1} for PCMC (i.e., 13.47 mmol reactive groups g^{-1}). For PAC the maximum sorption capacities (varying with the temperature) are in the range 0.58–0.77 mmol La g^{-1} while for PCMC they vary between 0.96 and 1.27 mmol La g^{-1}: this means that the maximum sorption capacities are about 66% higher for PCMC than for PAC while

Table 4
Thermodynamic parameters for the sorption of La(III) using Cellulose, PAC and PCMC.

Sorbent	Temperature (K)	ΔH° (kJ mol^{-1})	ΔS° (J mol^{-1} K^{-1})	ΔG° (kJ mol^{-1})	$T \times \Delta S^\circ$ (kJ mol^{-1})
Cellulose	293	3.18	88.4	−22.7	25.9
	300			−23.3	26.5
	313			−24.5	27.7
	323			−25.4	28.6
PAC	293	3.94	92.7	−23.2	27.2
	300			−23.9	27.8
	313			−25.1	29.0
	323			−26.0	30.0
PCMC	293	3.07	92.9	−24.2	27.2
	300			−24.8	27.9
	313			−26.0	29.1
	323			−26.9	30.0

the total number of reactive groups were about 77% greater for PCMC (compared to PAC). In the case of La(III) binding on diethylenetriaminepentaacetic acid (DTPA) immobilized on magnetite nanoparticles the metal occurs by interaction with 4 available acetate groups (with possible contribution of amino groups) (Almeida & Toma, 2016). Though the steric hindrance and conformation of reactive groups are different, assuming the same theoretical molar ratio would lead to a two-fold increase in the maximum sorption capacity compared to the actual results; this means that some reactive groups are probably not available or accessible.

Table 3 reports La(III) sorption performances of a series of sorbents. The comparison with the sorbents investigated in this study (though not exactly under the same experimental conditions) shows that PAC have comparable sorption capacities to conventional sorbents while PCMC is among the best sorbents. Though some of these selected materials have faster kinetics (Karnio et al., 2008) or higher sorption capacities (Chen, 2010), PCMC appears to be a competitive sorbent for La(III) recovery. Some resins, for example the gel-type weak acid resin GTWAR 110-H, exhibit even much higher sorption (i.e., 323 mg La g^{-1} at pH 5) (Xiong & Rao, 2012).

The Dubinin–Radushkevich (D–R) model was also used for fitting sorption isotherms. Fig. AM12 (see Additional Material Section) shows the linearization of experimental data. It is noteworthy that the plots were not linear when all the concentration data were used for the linearization (see example given by grey line linear correlation). Such a bad linearization would underestimate the slope and affect the determination of intrinsic parameters of the D–R model. The lowest metal concentration point was systematically removed from the linearization calculation giving good determination coefficients (R^2). Table AM3 (see Additional Material Section) shows the parameters for D–R modeling (calculations made on selected data removing the first concentration which is out of the linear range); it is noteworthy that the q_{DR} values obtained are very close to the experimental values and sorption capacities at monolayer saturation obtained with the Langmuir equation (Table 2): this justifies the conditions selected for D-R modeling. The E_{DR} values (mean free energy for sorption per mole) are systematically lower than 6.8 kJ mol^{-1}. It is commonly accepted that E_{DR} below 8 kJ mol^{-1} means that the sorption occurs through a physical sorption mechanism.

The Van't Hoff equation was used for calculating the thermodynamic parameters (Table 4 and Fig. 4) using the affinity coefficients of the Langmuir equation (i.e., b) obtained at different temperatures:

$$ln(b) = \frac{-\Delta S^0}{R} + \frac{-\Delta H^0}{R}\frac{1}{T} \quad (4)$$

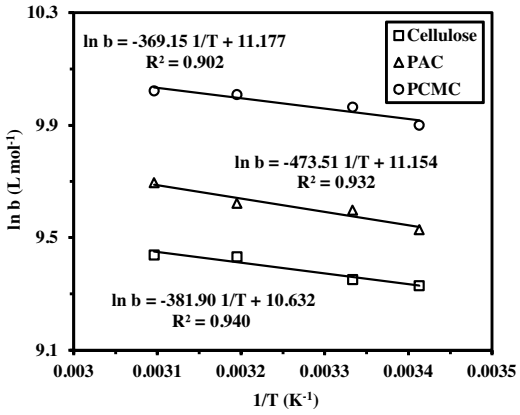

Fig. 4. Van't Hoff plot for La(III) sorption isotherms using Cellulose, PAC and PCMC (data from Fig. 3 and Table 2).

$$\Delta G^0 = \Delta H^0 - T\Delta S^0 \quad (5)$$

where ΔG^0 (kJ mol^{-1}), ΔH^0 (kJ mol^{-1}) and ΔS^0 (J mol^{-1} K^{-1}) are the free Gibbs energy change, the enthalpy change and the entropy change and R the gas constant (4.185 J mol^{-1} K^{-1}).

Table 4 shows that (a) the values of enthalpy change are positive (as a confirmation of the endothermic nature of the sorption process), and (b) very close for the three sorbents (ranging between 3.1 and 3.9 kJ mol^{-1}). The global enthalpy changes consist of the combination of the dehydration enthalpy (ΔH_{dehydr}, which is supposed to be positive due to the energy required for breaking the ion-water and water–water bonding of the hydrated metal ions) and the complexation enthalpy ($\Delta H_{complex}$, also positive) (Mahfouz, Killa, Sheta, Moustafa, & Tolba, 2014). The free Gibbs energy change is negative for the three sorbents (with values very close) the reaction is spontaneous (ΔG^0 absolute value increases with temperature). The entropy change was systematically positive: the randomness of the reaction increases with the sorption process. This may be associated to the release of water molecules bound to La(III) ions or the exchange of metal ions with more mobile ions (initially present on the sorbent) (Sert et al., 2008); the values are of the same order of magnitude than those found for lanthanum sorption on bamboo charcoal (Chen, 2010). In addition, $|T\Delta S^0| > |\Delta H^0|$; this means that the sorption process is more controlled by entropic changes than by enthalpy changes.

3.5. La(III) desorption and sorbent recycling

Metal desorption and sorbent recycling are key parameters for the competitiveness of the process: making possible the enrichment of the metal for further valorization, decreasing the cost of the process (by sorbent re-use), and in some cases metal desorption can be used for enhancing the selective separation of the metals (Nishihama et al., 2013; Raju, Srinivasan, & Subramanian, 2005). Nitric acid solutions (0.5 M) were used for eluting La(III) from metal-loaded sorbents. Table AM4 (see Additional Material Section) reports the sorption capacities obtained along 5 successive cycles of sorption/desorption. The three sorbents show a relatively good stability in sorption performance: the progressive decrease in sorption capacity does not exceed 8% for Cellulose and PCMC and 6% for PAC at the fifth cycle. Similar limited decrease in sorption efficiency was cited in the case of La(III) sorption/desorption from *Turbinaria conoides* macro alga (using 0.05 M HCl solutions) (Vijayaraghavan, Sathishkumar, & Balasubramanian, 2010). The sorbents can be efficiently recycled for a minimum of 5 cycles of sorption/desorption.

4. Conclusion

The grafting of tetraethylenepentamine on cellulose (TEPA) (via the chlorination of biopolymer backbone) produced a first sorbent (PAC) which can be functionalized by carboxymethylation (using monochloroacetic acid) to produce PCMC (a derivative of cellulose bearing both amino and carboxylic acid groups). FTIR analysis and acid-base titration confirmed the expected structures of the materials that are less crystalline than pristine cellulose. Sorption efficiency increases significantly above pH 3 due to the progressive deprotonation of carboxylic acids and protonated amine groups. The sorbents have increased efficiency for La(III) recovery following the sequence Cellulose « PAC < PCMC. Sorption is endothermic (positive ΔH^0), spontaneous (negative ΔG^0) and controlled by entropic change (positive ΔS^0) with sorption capacities reaching 38, 101 and 170 mg La g^{-1} for cellulose, PAC and PCMC, respectively. Langmuir equation fits well sorption isotherms and the uptake kinetics are controlled by the resistance to intraparticle diffusion. Indeed, the multi-linear plots with Weber and Morris equation mean that several mechanisms are involved depending on the co-existence of different pore sizes, the contribution of film diffusion, etc. However, the pseudo-first order rate equation perfectly fits kinetic profiles with apparent rate coefficients that are very similar for the three sorbents. Metal ions can be readily desorbed using 0.5 M HCl solutions and the decrease in sorption capacity remains below 8% at the fifth cycle. This makes these sorbents (especially PCMC) very efficient for La(III) recovery for environmental or valorization applications (metal recovery of valuable metals such as REEs). However, these materials could be also used as supports for other analytical applications or separation processes. Indeed, lanthanum can be immobilized on supports for synthesizing sorbents (immobilized metal-ion affinity chromatography, IMAC) with specific affinity for fluoride (Wang, Lin, Luo, & Yao, 2015; Zhang, Lyu, Su, Bian, Yu, & Zhang, 2016), phosphate (Wang, Liu, Liu et al., 2015; Wang, Shen, Shen, & Li, 2016) proteins (Liu, Zhang, Chen, & Wang, 2014), for example.

Acknowledgements

This work was supported by the International Atomic Energy Agency for financial support (IAEA for TC project number (Oracle Project No.: 1060242) and Fellowship Code No.: C6/EGY/15019). Authors acknowledge Eng. Thierry Vincent (Ecole des mines Alès, France) for ICP-AES analysis, Mrs Monmoko Iwai (chemist), (Hosei University, Japan) for CHN analysis, Dr. Yoshitomo Harada (Hosei University, Japan) for SEM-EDX and XPS analysis. Special dedication to the memory of Prof. Dr. Ahmed Donia.

References

Almeida, S. D. N., & Toma, H. E. (2016). Neodymium(III) and lanthanum(III) separation by magnetic nanohydrometallurgy using DTPA functionalized magnetite nanoparticles. *Hydrometallurgy*, *161*, 22–28.

Awwad, N. S., Gad, H. M. H., Ahmad, M. I., & Aly, H. F. (2010). Sorption of lanthanum and erbium from aqueous solution by activated carbon prepared from rice husk. *Colloids and Surfaces B—Biointerfaces*, *81*(2), 593–599.

Baba, Y., Kubota, F., Kamiya, N., & Goto, M. (2011). Selective recovery of dysprosium and neodymium ions by a supported liquid membrane based on ionic liquids. *Solvent Extraction Research and Development—Japan*, *18*, 193–198.

Binnemans, K., Jones, P. T., Blanpain, B., Van Gerven, T., Yang, Y., Walton, A., et al. (2013). Recycling of rare earths: A critical review. *Journal of Cleaner Production*, *51*, 1–22.

Borra, C. R., Pontikes, Y., Binnemans, K., & Van Gerven, T. (2015). Leaching of rare earths from bauxite residue (red mud). *Minerals Engineering*, *76*, 20–27.

Cadogan, E. I., Lee, C.-H., Popuri, S. R., & Lin, H.-Y. (2014). Efficiencies of chitosan nanoparticles and crab shell particles in europium uptake from aqueous solutions through biosorption: Synthesis and characterization. *International Biodeterioration & Biodegradation*, *95*, 232–240.

Cadogan, E. I., Lee, C.-H., & Popuri, S. R. (2015). Facile synthesis of chitosan derivatives and *Arthrobacter* sp. biomass for the removal of europium(III) ions from aqueous solution through biosorption. *International Biodeterioration & Biodegradation*, *102*, 286–297.

Charalampides, G., Vatalis, K. I., Apostoplos, B., & Ploutarch-Nikolas, B. (2015). Rare earth elements: Industrial applications and economic dependency of Europe. *Procedia Economics and Finance*, *24*, 126–135.

Chen, Q. (2010). Study on the adsorption of lanthanum(III) from aqueous solution by bamboo charcoal. *Journal of Rare Earths*, *28*, 125–131.

Ciolacu, D., Ciolacu, F., & Popa, V. I. (2011). Amorphous cellulose—Structure and characterization. *Cellulose Chemistry and Technology*, *45*(1–2), 13–21.

Coates, J. (2000). Interpretation of infrared spectra, a practical approach. In R. A. Meyers (Ed.), *Encyclopedia of analytical chemistry* (pp. 10815–10837). Chichester, U.K: John Wiley & Sons Ltd.

Das, N., & Das, D. (2013). Recovery of rare earth metals through biosorption: An overview. *Journal of Rare Earths*, *31*(10), 933–943.

De Stefano, C., Foti, C., Gianguzza, A., & Sammartano, S. (2000). Speciation of low molecular weight ligands in natural fluids: Protonation constants and association of open chain polyamines with the major components of seawater? *Analytica Chimica Acta*, *418*(1), 43–51.

Di Bernardo, P., Zanonato, P. L., Melchior, A., Portanova, R., Tolazzi, M., Choppin, G. R., et al. (2008). Thermodynamic and spectroscopic studies of lanthanides(III) complexation with polyamines in dimethyl sulfoxide. *Inorganic Chemistry*, *47*(3), 1155–1164.

Diniz, V., & Volesky, B. (2005a). Biosorption of La: Eu and Yb using *Sargassum* biomass. *Water Research*, *39*(1), 239–247.

Diniz, V., & Volesky, B. (2005b). Effect of counterions on lanthanum biosorption by *Sargassum polycystum*. *Water Research*, *39*(11), 2229–2236.

Dubinin, M. M., Zaverina, E. D., & Radushkevich, L. V. (1947). Sorption and structure of active carbons: I. Adsorption of organic vapors. *Zhurnal Fizicheskoi Khimii*, *21*, 1351–1362.

Dubois, M. A., Dozol, J. F., Nicotra, C., Serose, J., & Massiani, C. (1995). Pyrolysis and incineration of cationic and anionic ion-exchange resins—Identification of volatile degradation compounds. *Journal of Analytical and Applied Pyrolysis*, *31*, 129–140.

da Silva Filho, E. C., de Melo, J. C. P., & Airoldi, C. (2006). Preparation of ethylenediamine-anchored cellulose and determination of thermochemical data for the interaction between cations and basic centers at the solid/liquid interface? *Carbohydrate Research*, *341*(17), 2842–2850.

da Silva Filho, E. C., de Melo, J. C. P., da Fonseca, M. G., & Airoldi, C. (2009). Cation removal using cellulose chemically modified by a Schiff base procedure applying green principles. *Journal of Colloid and Interface Science*, *340*(1), 8–15.

Esma, B., Omar, A., & Amine, D. M. (2014). Comparative study on lanthanum(III) sorption onto lewatit TP 207 and lewatit TP 260. *Journal of Radioanalytical and Nuclear Chemistry*, *299*(1), 439–446.

Foo, K. Y., & Hameed, B. H. (2010). Insights into the modeling of adsorption isotherm systems. *Chemical Engineering Journal*, *156*(1), 2–10.

Freundlich, H. M. F. (1906). Uber die adsorption in lasungen. *Zeitschrift für Physikalische Chemie*, *57*, 385–470.

Galhoum, A. A., Mafhouz, M. G., Abdel-Rehem, S. T., Gomaa, N. A., Atia, A. A., Vincent, T., et al. (2015). Cysteine-functionalized chitosan magnetic nano-based particles for the recovery of light and heavy rare earth metals: Uptake kinetics and sorption isotherms? *Nanomaterials*, *5*(1), 154–179.

Galhoum, A. A., Mahfouz, M. G., Abdel-Rehem, S. T., Gomaa, N. A., Atia, A. A., Vincent, T., et al. (2015). Diethylenetriamine-functionalized chitosan magnetic nano-based particles for the sorption of rare earth metal ions Nd(III), Dy(III) and Yb(III). *Cellulose*, *22*(4), 2589–2605.

Galhoum, A. A., Atia, A. A., Mahfouz, M. G., Abdel-Rehem, S. T., Gomaa, N. A., Vincent, T., et al. (2015). Dy(III) recovery from dilute solutions using magnetic-chitosan nano-based particles grafted with amino acids? *Journal of Materials Science*, *50*(7), 2832–2848.

Galhoum, A. A., Mahfouz, M. G., Atia, A. A., Abdel-Rehem, S. T., Gomaa, N. A., Vincent, T., et al. (2015). Amino acid functionalized chitosan magnetic nanobased particles for uranyl sorption. *Industrial & Engineering Chemistry Research*, *54*(49), 12374–12385.

Gardner, S. D., Singamsetty, C. S. K., He, G. R., & Pittman, C. U. (1997). Chemical bonding of tetraethylenepentamine to nitric acid-oxidized carbon fibers: An XPS/ISS investigation? *Applied Spectroscopy*, *51*(5), 636–648.

Guzman, J., Saucedo, I., Navarro, R., Revilla, J., & Guibal, E. (2002). Vanadium interactions with chitosan: Influence of polymer protonation and metal speciation. *Langmuir*, *18*(5), 1567–1573.

Guzman, J., Saucedo, I., Revilla, J., Navarro, R., & Guibal, E. (2003). Copper sorption by chitosan in the presence of citrate ions: Influence of metal speciation on sorption mechanism and uptake capacities. *International Journal of Biological Macromolecules*, *33*(1–3), 57–65.

Hakim, L., Sabarudin, A., Oshima, M., & Motomizu, S. (2007). Synthesis of novel chitosan resin derivatized with serine diacetic acid moiety and its application to on-line collection/concentration of trace elements and their determination using inductively coupled plasma-atomic emission spectrometry? *Analytica Chimica Acta*, *588*(1), 73–81.

Ho, Y. S., & McKay, G. (1999). Pseudo-second order model for sorption processes. *Process Biochemistry*, *34*(5), 451–465.

Hong, G., Shen, L., Wang, M., Yang, Y., Wang, X., Zhu, M., et al. (2014). Nanofibrous polydopamine complex membranes for adsorption of lanthanum (III) ions. *Chemical Engineering Journal*, *244*, 307–316.

Hou, H., Xu, J., Wang, Y., & Chen, J. (2016). Solvent extraction of lanthanum and cerium ions from hydrochloric acidic aqueous solutions using partly saponified 2-ethylhexyl phosphonic acid mono-2-ethylhexyl ester? *Chinese Journal of Chemical Engineering*, *24*(1), 79–85.

Inoue, K., Ohto, K., Yoshizuka, K., Shinbaru, R., & Kina, K. (1995). Adsorption behaviors of some metal-ions on chitosan modified with EDTA-type ligand. *Bunseki Kagaku*, *44*(4), 283–287.

Isogai, A., Usuda, M., Kato, T., Uryu, T., & Atalla, R. H. (1989). Solid-state CP/MAS carbon-13 NMR study of cellulose polymorphs. *Macromolecules*, *22*(7), 3168–3172.

Jain, V. K., Handa, A., Pandya, R., Shrivastav, P., & Agrawal, Y. K. (2002). Polymer supported calixarene-semicarbazone, arene-semicarbazone derivative for separation and preconcentration of La(III), Ce(III), Th(IV) and U(VI). *Reactive and Functional Polymers*, *51*(2–3), 101–110.

Jain, V. K., Pandya, R. A., Pillai, S. G., Agrawal, Y. K., & Kanaiya, P. H. (2007). Solid-phase extractive preconcentration and separation of lanthanum(III) and cerium(III) using a polymer-supported chelating calix 4 arene resin. *Journal of Analytical Chemistry*, *62*(2), 104–112.

Karnio, E., Fujiwara, Y., Mats Urnoto, M., Valenzuela, F., & Kondo, K. (2008). Investigation on extraction rate of lanthanides with extractant-impregnated microcapsule. *Chemical Engineering Journal*, *139*(1), 93–105.

Karve, M., & Rajgor, R. V. (2008). Amberlite XAD-2 impregnated organophosphinic acid extractant for separation of uranium(VI) from rare earth elements. *Desalination*, *232*(1–3), 191–197.

Kazy, S. K., Das, S. K., & Sar, P. (2006). Lanthanum biosorption by a *Pseudomonas* sp.: Equilibrium studies and chemical characterization. *Journal of Industrial Microbiology & Biotechnology*, *33*(9), 773–783.

Koto, Y., Kano, N., Wang, Y., Sakamoto, N., & Imaizumi, H. (2010). Biosorption of lanthanides from aqueous solutions using pretreated *Buccinum tenuissimum* shell biomass. *Bioinorganic Chemistry and Applications*, *2010*, 10p. http://dx.doi.org/10.1155/2010/804854. Article ID 804854

Krishnaveni, R., & Thambidurai, S. (2011). Effect of solvents on cyanoethylation of cotton cellulose and its properties. *Journal of Applied Polymer Science*, *122*(3), 1622–1627.

Lagergren, S. (1898). About the theory of so-called adsorption of soluble substances. *Kungliga Svenska Vetenskapsakademiens*, *24*, 1–39.

Langmuir, I. (1918). The adsorption of gases on plane surfaces of glass, mica and platinum. *Journal American Chemical Society*, *40*, 1361–1402.

Liu, S. L., & Zhang, L. N. (2009). Effects of polymer concentration and coagulation temperature on the properties of regenerated cellulose films prepared from LiOH/urea solution. *Cellulose*, *16*(2), 189–198.

Liu, J. W., Zhang, Y., Chen, X. W., & Wang, J. H. (2014). Graphene oxide-rare earth metal-organic framework composites for the selective isolation of hemoglobin? *ACS Applied Materials & Interfaces*, *6*(13), 10196–10204.

Lo, T. C., Baird, M. H. I., & Hanson, C. (1991). *Handbook of solvent extraction*. Malabar, Florida (U.S.A.): Krieger Publishing Company.

Lo, Y. C., Cheng, C. L., Han, Y. L., Chen, B. Y., & Chang, J. S. (2014). Recovery of high-value metals from geothermal sites by biosorption and bioaccumulation. *Bioresource Technology*, *160*, 182–190.

Maheswari, M. A., & Subramanian, M. S. (2004). Selective enrichment of U(VI), Th(IV) and La(III) from high acidic streams using a new chelating ion-exchange polymeric matrix. *Talanta*, *64*(1), 202–209.

Mahfouz, M. G., Killa, H. M., Sheta, M. E., Moustafa, A. H., & Tolba, A. A. (2014). Synthesis, characterization, and application of polystyrene adsorbents containing tri-n-butylphosphate for solid-phase extraction of uranium (VI) from aqueous nitrate solutions. *Journal of Radioanalytical and Nuclear Chemistry*, *301*(3), 739–749.

Mahfouz, M. G., Galhoum, A. A., Gomaa, N. A., Abdel-Rehem, S. S., Atia, A. A., Vincent, T., et al. (2015). Uranium extraction using magnetic nano-based particles of diethylenetriamine-functionalized chitosan: Equilibrium and kinetic studies. *Chemical Engineering Journal*, *262*, 198–209.

Marcus, Y. (1997). *Ion properties*. New York, NY: Marcel Dekker, Inc.

Martsul, V. N., & Kozlowskaya, I. Y. (2015). Recovery of lanthanum from acid leaching solutions of spent cracking catalyst? *Russian Journal of Applied Chemistry*, *88*(10), 1589–1593.

Nishihama, S., Kohata, K., & Yoshizuka, K. (2013). Separation of lanthanum and cerium using a coated solvent-impregnated resin. *Separation and Purification Technology*, *118*, 511–518.

O'Connell, D. W., Aszalos, B., Birkinshaw, C., & O'Dwyer, T. F. (2010). A study of the mechanisms of divalent copper binding to a modified cellulose adsorbent. *Journal of Applied Polymer Science*, *116*(5), 2496–2503.

Oh, S. Y., Yoo, D. I., Shin, Y., Kim, H. C., Kim, H. Y., Chung, Y. S., et al. (2005). Crystalline structure analysis of cellulose treated with sodium hydroxide and carbon dioxide by means of X-ray diffraction and FTIR spectroscopy. *Carbohydrate Research*, *340*(15), 2376–2391.

Oliveira, R. C., Guibal, E., & Garcia, O., Jr. (2012). Biosorption and desorption of lanthanum(III) and neodymium(III) in fixed-bed columns with *Sargassum* sp.: Perspectives for separation of rare earth metals. *Biotechnology Progress*, *28*(3), 715–722.

Ozaki, T., Suzuki, Y., Nankawa, T., Yoshida, T., Ohnuki, T., Kimura, T., et al. (2006). Interactions of rare earth elements with bacteria and organic ligands. *Journal of Alloys and Compounds*, *408*, 1334–1338.

Park, S., Baker, J. O., Himmel, M. E., Parilla, P. A., & Johnson, D. K. (2010). Cellulose crystallinity index: Measurement techniques and their impact on interpreting cellulase performance. *Biotechnology for Biofuels*, *3*

Pearson, R. G. (1966). Acids and bases. *Science (New York, N.Y.)*, *151*(3707), 172–177.

Puigdomenech, I. (2010). *MEDUSA (make equilibrium diagrams using sophisticated algorithms)*. Stockholm, Sweden: Royal Institute of Technology.

Rahman, M. M., Khan, S. B., Marwani, H. M., & Asiri, A. M. (2014). SnO_2-TiO_2 nanocomposites as new adsorbent for efficient removal of La(III) ions from aqueous solutions? *Journal of the Taiwan Institute of Chemical Engineers*, *45*(4), 1964–1974.

Raju, C. S. K., Srinivasan, S., & Subramanian, M. S. (2005). New multi-dentate ion-selective AXAD-16-MOPPA polymer for the preconcentration and sequential separation of U(VI), Th(IV) from rare earth matrix. *Separation Science and Technology*, *40*(11), 2213–2230.

Repo, E., Warchol, J. K., Bhatnagar, A., Mudhoo, A., & Sillanpaa, M. (2013). Aminopolycarboxylic acid functionalized adsorbents for heavy metals removal from water? *Water Research*, *47*(14), 4812–4832.

Roosen, J., & Binnemans, K. (2014). Adsorption and chromatographic separation of rare earths with EDTA- and DTPA-functionalized chitosan biopolymers. *Journal of Materials Chemistry A*, *2*(5), 1530–1540.

Roosen, J., Spooren, J., & Binnemans, K. (2014). Adsorption performance of functionalized chitosan-silica hybrid materials toward rare earths? *Journal of Materials Chemistry A*, *2*(45), 19415–19426.

Sert, Ş., Kütahyali, C., İnan, S., Talip, Z., Çetinkaya, B., & Eral, M. (2008). Biosorption of lanthanum and cerium from aqueous solutions by *Platanus orientalis* leaf powder. *Hydrometallurgy*, *90*(1), 13–18.

Sharma, P. R., & Varma, A. J. (2014). Thermal stability of cellulose and their nanoparticles: Effect of incremental increases in carboxyl and aldehyde groups. *Carbohydrate Polymers*, *114*, 339–343.

Shen, H. Y., Chen, J. L., Dai, H. F., Wang, L. B., Hu, M. Q., & Xia, Q. H. (2013). New insights into the sorption and detoxification of chromium(VI) by tetraethylenepentamine functionalized nanosized magnetic polymer adsorbents: Mechanism and pH effect. *Industrial & Engineering Chemistry Research*, *52*(36), 12723–12732.

Silva Filho, E. C., Lima, L. C. B., Silva, F. C., Sousa, K. S., Fonseca, M. G., & Santana, S. A. A. (2013). Immobilization of ethylene sulfide in aminated cellulose for removal of the divalent cations. *Carbohydrate Polymers*, *92*(2), 1203–1210.

Sinha, S., Abhilash, Meshram, P., & Pandey, B. D. (2016). Metallurgical processes for the recovery and recycling of lanthanum from various resources—A review. *Hydrometallurgy*, *160*, 47–59.

Song, D., Park, S.-J., Kang, H. W., Park, S. B., & Han, J.-I. (2013). Recovery of lithium(I) strontium(II), and lanthanum(III) using Ca-alginate beads. *Journal of Chemical and Engineering Data*, *58*(9), 2455–2464.

Stenstad, P., Andresen, M., Tanem, B. S., & Stenius, P. (2008). Chemical surface modifications of microfibrillated cellulose. *Cellulose*, *15*(1), 35–45.

Sun, X., Ji, Y., Chen, J., & Ma, J. (2009). Solvent impregnated resin prepared using task-specific ionic liquids for rare earth separation. *Journal of Rare Earths*, *27*(6), 932–936.

Sun, X., Chi-Linh, D.-T., Luo, H., & Dai, S. (2014). The optimization of an ionic liquid-based TALSPEAK-like process for rare earth ions separation. *Chemical Engineering Journal*, *239*, 392–398.

Tashiro, T., & Shimura, Y. (1982). Removal of mercuric ions by systems based on cellulose derivatives. *Journal of Applied Polymer Science*, *27*(2), 747–756.

Texier, A. C., Andres, Y., Illemassene, M., & Le Cloirec, P. (2000). Characterization of lanthanide ions binding sites in the cell wall of *Pseudomonas aeruginosa*. *Environmental Science & Technology*, *34*(4), 610–615.

Torab-Mostaedi, M., Asadollahzadeh, M., Hemmati, A., & Khosravi, A. (2013). Biosorption of lanthanum and cerium from aqueous solutions by grapefruit peel: Equilibrium, kinetic and thermodynamic studies. *Research on Chemical Intermediates*, *41*(2), 559–573.

Tunsu, C., Petranikova, M., Ekberg, C., & Retegan, T. (2016). A hydrometallurgical process for the recovery of rare earth elements from fluorescent lamp waste fractions. *Separation and Purification Technology*, *161*, 172–186.

Vander Hoogerstraete, T., & Binnemans, K. (2014). Highly efficient separation of rare earths from nickel and cobalt by solvent extraction with the ionic liquid trihexyl(tetradecyl) phosphonium nitrate: A process relevant to the recycling of rare earths from permanent magnets and nickel metal hydride batteries. *Green Chemistry*, *16*(3), 1594–1606.

Vigo, T. L., & Welch, C. M. (1974). Chlorination and phosphorylation of cotton cellulose by reaction with phosphoryl chloride in *N*,*N*-dimethylformamide. *Carbohydrate Research*, *32*(2), 331–338.

Vijayaraghavan, K., Sathishkumar, M., & Balasubramanian, R. (2010). Biosorption of lanthanum, cerium, europium, and ytterbium by a brown marine alga, Turbinaria conoides. *Industrial & Engineering Chemistry Research*, *49*(9), 4405–4411.

Wang, L. C., Chen, X. G., Liu, C. S., Li, P. W., & Zhou, P. M. (2008). Dissociation behaviors of carboxyl and amine groups on carboxymethyl-chitosan in aqueous system. *Journal of Polymer Science Part B—Polymer Physics*, *46*(14), 1419–1429.

Wang, Z., Shen, D., Shen, F., & Li, T. (2016). Phosphate adsorption on lanthanum loaded biochar. *Chemosphere*, *150*, 1–7.

Wang, J., Lin, X., Luo, X., & Yao, W. (2015). Preparation and characterization of the linked lanthanum carboxymethylcellulose microsphere adsorbent for removal of fluoride from aqueous solutions? *RSC Advances*, *5*(73), 59273–59285.
Wang, X., Liu, Z., Liu, J., Huo, M., Huo, H., & Yang, W. (2015). Removing phosphorus from aqueous solutions using lanthanum modified pine needles. *Plos One*, *10*(12), e0142700.
Weber, W. J., & Morris, J. C. (1963). Kinetics of adsorption on carbon from solutions. *Journal of Sanitary Engineering Division ASCE*, *89*, 31–60.
Wu, D., Zhao, J., Zhang, L., Wu, Q., & Yang, Y. (2010). Lanthanum adsorption using iron oxide loaded calcium alginate beads. *Hydrometallurgy*, *101*(1–2), 76–83.
Wu, D., Zhang, L., Wang, L., Zhu, B., & Fan, L. (2011). Adsorption of lanthanum by magnetic alginate-chitosan gel beads? *Journal of Chemical Technology and Biotechnology*, *86*(3), 345–352.
Xiong, C., & Rao, C. (2012). Use of gel-type weak acid resin for the adsorption of La(III) from aqueous solution. *Indian Journal of Chemical Technology*, *19*(6), 392–398.
Ye, J., Wang, B., Xiong, J., & Sun, R. C. (2016). Enhanced fluorescence and structural characteristics of carboxymethyl cellulose/Eu(III) nano-complex: Influence of reaction time. *Carbohydrate Polymers*, *135*, 57–63.
Zhang, S., Lyu, Y., Su, X., Bian, Y., Yu, B., & Zhang, Y. (2016). Removal of fluoride ion from groundwater by adsorption on lanthanum and aluminum loaded clay adsorbent. *Environmental Earth Sciences*, *75*(5).
Zhu, Y., Wang, W., Zheng, Y., Wang, F., & Wang, A. (2016). Rapid enrichment of rare-earth metals by carboxymethyl cellulose-based open-cellular hydrogel adsorbent from HIPEs template. *Carbohydrate Polymers*, *140*, 51–58.